




## Temporal Variation of Soil Gas Radon Associated with Seismic Activity: A Case Study in NW Greece

C. PAPACHRISTODOULOU,<sup>1</sup>  K. STAMOULIS,<sup>1</sup> and K. IOANNIDES<sup>1</sup>

**Abstract**—Soil gas radon concentrations were continuously monitored from November 2016 to May 2018, close to an active fault zone in the area of Ioannina (Northwestern Greece) that gave rise to intense seismic swarms with magnitudes up to 5.3 on the Richter scale, during October 2016. Meteorologic parameters (soil and air temperature, atmospheric pressure, wind speed and rainfall) were simultaneously obtained, and their contribution to radon fluctuations was examined by partial correlation and cross-correlation analysis. Soil temperature and atmospheric pressure were found to be the parameters controlling radon concentrations, and their effect was reduced using multiple linear regression analysis. During the monitoring period, 11 spike-like anomalies were identified in the residual radon time series using the  $2\sigma$  deviation criterion. The duration of the anomalies varied from  $< 1$  day to approximately 5 days. Earthquakes of local magnitudes  $M_L > 2.5$ , occurring within a distance of 100 km from the monitoring site, were collected and filtered by applying Dobrovolsky's radius approach. Most of the observed radon anomalies were likely associated with seismic events, and the precursor time ranged roughly from 2 to 15 days.

**Key words:** Radon, time series, meteorologic parameters, earthquake, precursor, Greece.

### 1. Introduction

Radon ( $^{222}\text{Rn}$ ) is a naturally occurring radioactive gas produced in the Earth's crust by the  $^{238}\text{U}$  decay chain. Due to its high mobility, radon can leave rocks and soils, escaping toward the surface through fractures and openings, by a combination of diffusive and advective transport. Although diffusion is a short-scale mechanism limited by the radon half-life (3.82 days), advection can lead to transport over long distances, with radon being carried by rising fluids or gases (Kristiansson and Malmqvist 1982; Etiope and

Martinelli 2002). The latter mechanism is significantly accentuated by the stress-strain developed within the Earth's crust before an impending earthquake and results in anomalous changes in radon concentration that occur not only in the vicinity of the epicentral area, but also at much larger distances (Fleischer 1981; Hauksson and Goddard 1981; King 1986; Toutain and Baubron 1999).

Over the past decades, radon monitoring in soil and in ground- or springwater has shown that spatial and temporal radon variations can be exploited for earthquake predicting purposes. A wealth of worldwide compilations reviewing earthquake-related abnormal radon signals and physical models proposed for their interpretation is available in the literature (Toutain and Baubron 1999; Hartmann and Levy 2005; Cicerone et al. 2009; Ghosh et al. 2009; Immè and Morelli 2012; Petraki et al. 2015; Riggio and Santulin 2015; Woith 2015; Tomer 2016). Other than geophysical processes, meteorologic conditions—such as barometric pressure, temperature, soil humidity, wind and rainfall—influence radon concentration levels in soil, gas or water. The effect of atmospheric parameters on radon fluctuations should therefore be reduced before attempting to associate radon anomalies with seismic events (Singh et al. 1988; Igarashi and Wakita 1990; Matsumoto 1992; Zmazek et al. 2003; Jaishi et al. 2014; Kumar et al. 2015; Piersanti et al. 2016).

The identification of an anomaly in radon time series and the definition of the anomaly parameters—i.e., the duration, amplitude and precursor time—have been tackled by different researchers. A radon variation crossing the  $2\sigma$  confidence interval from the mean value at the monitoring site is typically identified as a significant anomaly (Hauksson and

<sup>1</sup> Department of Physics, University of Ioannina, 451 10 Ioannina, Greece. E-mail: xpapaxri@uoi.gr

Goddard 1981; Igarashi and Wakita 1990; Virk et al. 2002; Zmazek et al. 2005; Ghosh et al. 2011; Gregorič et al. 2012). More sophisticated methods, involving artificial neural networks, regression and decision tree models, have been applied to predict the effect of meteorologic variables and isolate radon fluctuations solely driven by geophysical phenomena (Negarestani et al. 2003; Zmazek et al. 2003; Sikder and Munakata 2009; Torkar et al. 2010).

In the present study, the temporal variability of soil gas radon was continuously monitored from November 2016 to May 2018 near a seismically active location in the area of Ioannina (Epirus, Northwestern Greece). The monitoring site was within 25 km of the fault zone that gave rise to intense seismic swarms with magnitudes up to 5.3 on the Richter scale during October 2016. The quakes were distinctly felt by the population, and the news was reported by the major national media. The aim of the study was to identify radon anomalies possibly associated with the seismic activity in the area. To this end, the fluctuations of atmospheric/soil meteorologic parameters were also obtained and analyzed to account for their effect on radon time series. The residual radon concentrations were subsequently correlated with earthquake events recorded during the selected time window, and the results are compared with earlier findings reported in the published literature.

## 2. Geotectonics of the Study Area

The region of Epirus, Northwestern Greece, features a complex geologic structure characterized by a sharp relief and abundant surface water bodies. It is delimited to the west by the Ionian Sea and to the south by the Gulf of Arta, while its northern and eastern boundaries are defined by the Pindos mountain range with elevations exceeding 2000 m. The land between the Ionian coast and Pindos Mountains is traversed by a succession of ridges, composed of Mesozoic carbonates, with typical elevations between 1200 and 1700 m, separated by narrow plains (King et al. 1993). Four major rivers constitute the drainage network of Epirus: the Kalamas and Acheron Rivers, which reach the Ionian Sea, and the Louros and

Arachthos Rivers, which drain into the Gulf of Arta. The Ioannina basin is situated toward the eastern side of the region and contains Pamvotis Lake with a history going back into the Pliocene.

The dominant geotectonic zones that develop in the area, overthrusting one another, are—from east to west—the Subpelagonian (4.4% of the total area), the Pindos (12%), the Gavrovo (5.6%) and the Ionian (78%) zone (Aubouin 1959; Ntokos 2017a). Reverse, normal and strike-slip faults have influenced the geologic formations of these geotectonic zones. The western part of the region is dominated by reverse and strike-slip faults, resulting from compressive stresses of the NE-SW to ENE-WSW direction. Normal and oblique-slip faults are primarily encountered in the eastern part because of the major presence of extensive stresses, generally trending NW-SE (Ntokos 2017a, b). The main active faults of Epirus—i.e., tectonic structures that were either formed or re-activated from the Upper Pleistocene until the present (aged < 120,000 years), having a potential for future activation (Pavlidis et al. 2008)—are shown in Fig. 1.

Based on instrumental earthquake records, the seismicity in the area features many low-magnitude seismic events (Hatzfeld et al. 1995; Tselentis et al. 2006) and a limited number of high magnitude seismic events (Papazachos and Papazachou 1989). The spatial distribution of the epicenters is scattered, showing no clear seismotectonic correlation between specific faults and seismic activity (Boccaletti et al. 1997). Concerning the most recent seismic activity, the earthquake of 15 October 2016 ( $M_L = 5.3$ ) occurred at a depth of 17 km, with an epicenter of (39.79°N, 20.69°E), 19.4 km NW of the city of Ioannina. The earthquake was part of a geotectonic environment of lithospheric compression. By the end of that month, 65 minor to moderate aftershocks ( $3 < M_L < 4.9$ ) had been recorded by the Geodynamic Institute at Athens' National Observatory (<http://www.gein.noa.gr/>), their distribution pointing to the activation of a 10–12-km fault zone, striking NNW-SSE and dipping 26°–27° to the east (Pavlidis et al. 2016). Focal mechanism data provide indications for a high-angle reverse fault, which is believed to be either a secondary fault capable of producing  $M_L > 5$  earthquakes or a seismogenic segment of a

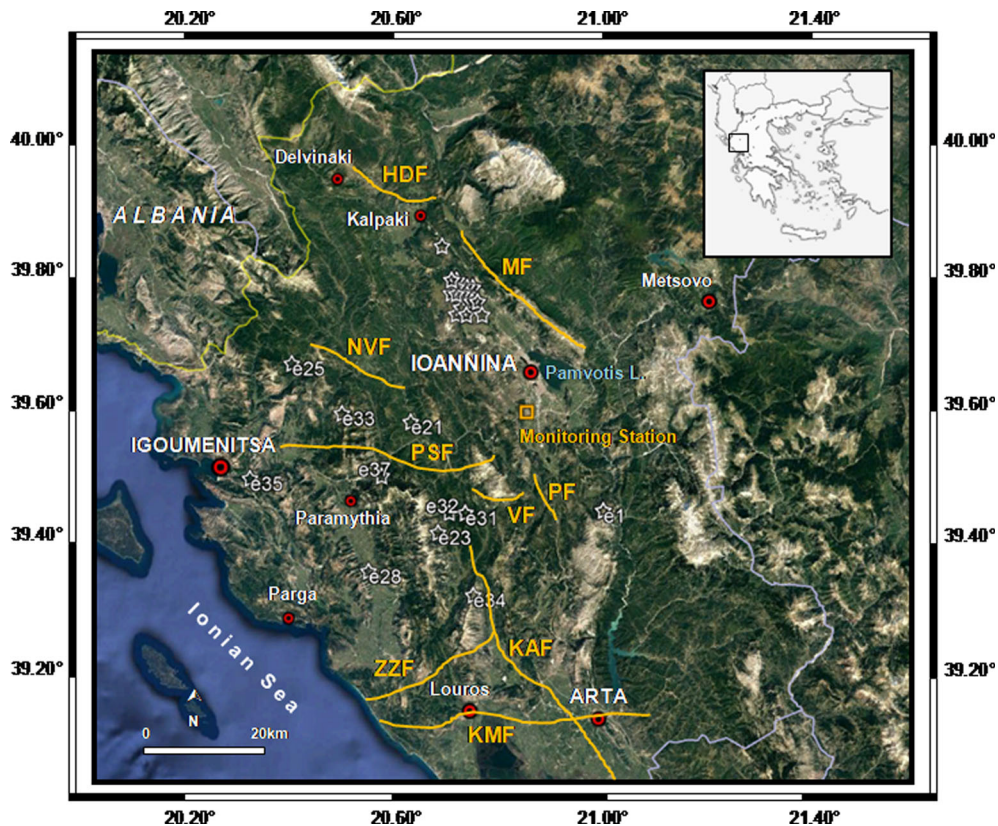


Figure 1

Map showing the study area and location of the monitoring station. Star symbols indicate the locations of the earthquakes listed in Table 1. Active faults were adopted from Ntokos (2018) and are illustrated by yellow lines. *HDF* Hani Delvinaki reverse strike-slip fault, *MF* Mitsikeli oblique-slip fault, *NVF* Nerochori-Vrosina strike-slip fault, *PSF* Petousi-Souli strike-slip fault, *VF* Variadhes strike-slip fault, *PF* Pesta oblique-slip fault, *KAF* Kokkinopilos-Arta strike-slip fault, *ZZF* Zalogo-Ziros oblique-slip fault, *KMF* Kamarina-Arta oblique-slip fault

larger fault or fault zone of a capacity comparable to the historical earthquakes in the region (Pavlidis et al. 2017). However, its precise determination requires the assessment of seismologic and geodetic data as well as the study of its seismic behavior.

From a geologic point of view, the Ioannina basin, which includes the monitoring site and fault zone that generated the October 2016 earthquake sequence, consists of alluvial and siliceous deposits, clays, tertiary flysch, limestones and dolomites (Aubouin 1959; Karakitsios 2005). The monitoring site (39.60°N, 20.84°E) was installed in the vicinity of Ioannina, within 25 km of the fault zone (Fig. 1). The top soil in the area was classified as a sandy loam on the basis of its grain size distribution, assessed through dry sieving (gravel 8%, coarse sand 18%, fine sand 43%, silt 22% and clay 9%). Mineralogic

analysis showed high amounts of quartz and calcite and small amounts of plagioclase feldspars, kaolinite and illite.

### 3. Materials and Methods

#### 3.1. Soil Gas Radon and Meteorologic Parameters

Soil radon concentrations were continuously measured by a Barasol MC2 multi-sensor (ALGADE, Bessines-sur-Gartempe, France), installed in the monitoring site. The detector was placed inside a PVC tube at a depth of 80 cm below the ground surface. The topsoil was covered with a polyethylene sheet to reduce penetration of rainwater in the tube. Radon gas diffuses through cellulose filters in the

Barasol measurement chamber (62 mm diameter, 489 mm length), and the detection of alpha particles is achieved through an implanted silicon junction, with an active area of 400 mm<sup>2</sup> and resolution of 60 keV (FWHM) at 5.486 MeV (<sup>241</sup>Am) in the air. The discrimination window is set from 0.7 to 6.1 MeV to eliminate any contribution from the electronic background noise and <sup>220</sup>Rn and to achieve a fast response from longer lived isotopes, such as <sup>214</sup>Po, <sup>212</sup>Po and <sup>212</sup>Bi deposited on the detector and chamber walls. The sensitivity is typically 0.02 counts h<sup>-1</sup> per Bq m<sup>-3</sup>, while the detection limit for radon is 50 Bq m<sup>-3</sup> and the detection range extends to 1 GBq m<sup>-3</sup>. Barasol totalizes alpha events detected during pre-established time intervals of 1–240 min, and data are stored in a micro-processor. Readout is performed by a PC-compatible computer with associated software. The probe also measures the soil temperature and atmospheric pressure with an accuracy of 0.1 °C and 1 mbar, respectively. The detector recorded data from November 2016 to May 2018, with a sampling interval of 1 h. A couple of disruptions occurred during the acquisition period because of the failure of the lithium batteries supplying the radon probe.

Daily air temperature, rainfall and wind speed data from a meteorologic station, installed 1 m above the ground surface at around 2 km from the radon monitoring site, were retrieved from the interactive database of the Institute for Environmental Research and Sustainable Development at Athens' National Observatory (<http://meteosearch.meteo.gr/>).

### 3.2. Earthquake Data

Earthquake data were collected from the Earthquake Data Base of the Geodynamic Institute at Athens' National Observatory (<http://www.gein.noa.gr/>). Earthquakes of magnitude  $M_L > 2.5$  occurring at an epicentral distance  $R_E < 100$  km from the monitoring site, with a focal depth  $< 50$  km, were considered in the analysis. To isolate those events that could generate soil radon anomalies at the monitoring site, the effective radius  $R_D$  (km), introduced by Dobrovolsky et al. (1979), was calculated using the formula:

$$R_D = 10^{0.43M_L}.$$

The  $R_D$  parameter defines the earthquake preparation zone, i.e., the area within which precursory phenomena may be observed. The condition  $R_E \leq 1.5R_D$  (Zmazek et al. 2005; Vaupotic et al. 2010; Walia et al. 2013; Oh and Kim 2015; Barkat et al. 2018) was subsequently applied to obtain the earthquake catalog listed in Table 1. Of the 192 seismic events initially obtained from the database, 37 earthquakes satisfied the above criteria; they were shallow seismic events (depth between 3 and 23 km) with magnitudes up to  $M_L = 3.8$ , mostly (67%) generated at the fault that gave rise to the October 2016 earthquake.

## 4. Results

The time series of soil radon concentration recorded from November 2016 to May 2018 along with soil and air meteorologic data are displayed in Fig. 2. The earthquake events listed in Table 1 are also marked. Power supply problems in the Barasol detector caused the loss of data from 10 December to 26 December 2016 and from 3 November 2017 to 3 January 2018.

Radon activities span from 1 to 80 kBq m<sup>-3</sup>. Several spike-like radon peaks appear from November 2016 to March 2017 and from January to May 2018, while more or less background fluctuations are observed from April to November 2017. A coarse look at the data suggests that the periods of radon spikes coincide with periods of frequent seismic events.

### 4.1. Influence of Meteorologic Parameters

Prior to identifying any radon anomalies possibly related to geodynamic processes, the effect of meteorologic parameters on radon time series has been thoroughly examined. As a first step, the hourly Barasol data of soil temperature ( $T_s$ ), atmospheric pressure ( $P$ ) and radon concentration (Rn) were studied by fast Fourier transform (FFT) analysis to compare the spectral components of the signals. Frequency spectra were obtained for the entire time

Table 1

*List of earthquakes ( $e_i$ ) recorded during the monitoring period (November 2016–May 2018)*

$e_i$	Date (dd.mm.yyyy hour)	Lat. (°N)	Long. (°E)	$M_L$	$R_E$ (km)	$D$ (km)	$R_E/R_D$	$a_i$	$t_a$ (dd.mm.yyyy h)	$t_p$ (days)	$D_t$ (days)
e1	10.11.2016 00:53:54	39.46	20.99	3	20.2	3	1.04	a1	7.11.2016 17:00	2.3	0.8
e2	11.11.2016 06:07:34	39.79	20.69	2.9	24.7	4	1.40				
e3	13.11.2016 22:52:06	39.78	20.73	2.9	22.1	8	1.25				
e4	15.11.2016 19:21:58	39.78	20.73	3.2	22.1	8	0.93				
e5	15.11.2016 20:32:52	39.78	20.70	2.8	23.3	4	1.46				
e6	16.11.2016 00:27:54	39.77	20.72	3	21.5	7	1.10				
e7	16.11.2016 00:55:45	39.78	20.71	3.1	22.9	13	1.06				
e8	16.11.2016 04:47:47	39.74	20.75	2.6	17.4	9	1.33				
e9	16.11.2016 08:49:14	39.76	20.73	2.9	20.1	8	1.14				
e10	16.11.2016 11:41:07	39.76	20.74	3.8	19.7	16	0.46	a2	12.11.2016 18:00	3.7	1.0
e11	17.11.2016 19:54:52	39.77	20.71	3.2	21.9	4	0.92				
e12	17.11.2016 20:23:30	39.78	20.72	3.3	22.5	7	0.86				
e13	17.11.2016 21:07:14	39.79	20.70	3.3	24.3	7	0.93				
e14	18.11.2016 17:41:27	39.77	20.69	3.2	22.8	5	0.96				
e15	18.11.2016 18:11:36	39.78	20.72	2.8	22.5	5	1.41				
e16	19.11.2016 04:29:12	39.76	20.74	3.1	19.7	6	0.92				
e17	15.12.2016 22:37:19	39.78	20.73	2.8	22.1	7	1.38		Missing radon data		
e18	19.12.2016 21:32:32	39.78	20.72	3.3	22.5	14	0.86		Missing radon data		
e19	30.12.2016 03:28:27	39.74	20.70	2.6	19.6	7	1.49		Missing radon data		
e20	31.12.2016 19:20:06	39.45	20.73	2.8	19.2	10	1.20		Missing radon data		
e21	9.01.2017 18:04:58	39.58	20.62	2.7	19.0	12	1.31				
e22	13.01.2017 17:24:35	39.74	20.72	2.9	18.7	9	1.06	a3	7.01.2017 15:00	6.1	1.5
e23	1.02.2017 15:51:12	39.42	20.68	2.7	20.3	8	1.40	a4	24.01.2017 06:00	8.9	0.7
								a5	29.01.2017 03:00	3.5	0.8
e24	13.02.2017 19:08:43	39.79	20.69	3	24.7	12	1.27	a6	3.02.2017 17:00	10.1	0.9
e25	24.02.2017 22:37:26	39.66	20.39	3.3	39.1	6	1.49	a7	16.2.2017 16:00	8.3	0.8
e26	15.03.2017 01:14:11	39.75	20.71	2.8	20.0	5	1.25				
e27	16.03.2017 03:00:58	39.74	20.72	3.3	18.7	6	0.71	a8	1.03.2017 11:00	14.7	0.7
e28	25.03.2017 19:53:00	39.36	20.55	3.5	36.5	18	1.14	–	–	–	–
e29	1.04.2017 23:46:33	39.77	20.70	3.4	22.4	9	0.77	a9	30.03.2017 07:00	2.7	1.1
e30	3.04.2017 19:32:24	39.79	20.70	3.1	24.3	8	1.13				
e31	20.10.2017 13:21:55	39.45	20.73	2.7	19.2	8	1.33	–	–	–	–
e32	25.11.2017 07:35:45	39.45	20.70	2.8	20.6	5	1.29		Missing radon data		
e33	12.02.2018 05:58:19	39.59	20.49	3.6	30.0	4	0.85	a11	1.02.2018 10:00	10.8	5.1
e34	27.03.2018 08:13:14	39.33	20.75	3.5	31.0	20	0.97	–	–	–	–
e35	6.04.2018 15:07:37	39.49	20.32	3.5	46.2	3	1.44	–	–	–	–
e36	15.04.2018 01:58:46	39.84	20.67	3.2	30.4	12	1.28	–	–	–	–
e37	23.05.2018 07:19:10	39.50	20.57	3	25.7	23	1.32	–	–	–	–

The geographical position, local magnitude ( $M_L$ ), epicentral distance from the monitoring site ( $R_E$ ) and focal depth ( $D$ ) of the earthquakes are included. Only the earthquakes complying with the selection criteria  $M_L > 2.5$ ,  $R_E < 100$  km,  $D < 50$  km and  $R_E \leq 1.5R_D$  are presented. The observed radon anomalies ( $a_i$ ) are indicated, including the time of occurrence ( $t_a$ ), precursor time ( $t_p$ ) and anomaly duration ( $D_t$ ), calculated as explained in Sect. 4.3

series, with a 1-h resolution, using a Hanning window (Fig. 3). The soil temperature spectrum exhibits a single 24-h periodicity, generated by diurnal variations, as indicatively shown in Fig. 4 for two different periods (winter and summer), which were free from radon peaks. The atmospheric pressure spectrum shows intense harmonics at 24 h and 12 h as well as a weak peak at 8 h. Such periodicities, reflecting the

S1, S2 and S3 tidal frequencies, are typically reported for atmospheric pressure variations (Mentes and Eper-Pápai 2015; Fu et al. 2017c). The diurnal component is also dominant in the radon spectrum, while weak peaks at 12 h and 8 h are also discernible. The S1 (24 h) and S2 (12 h) waves are indeed often detected in radon signals and interpreted as the result of diurnal temperature variations and barometric tides

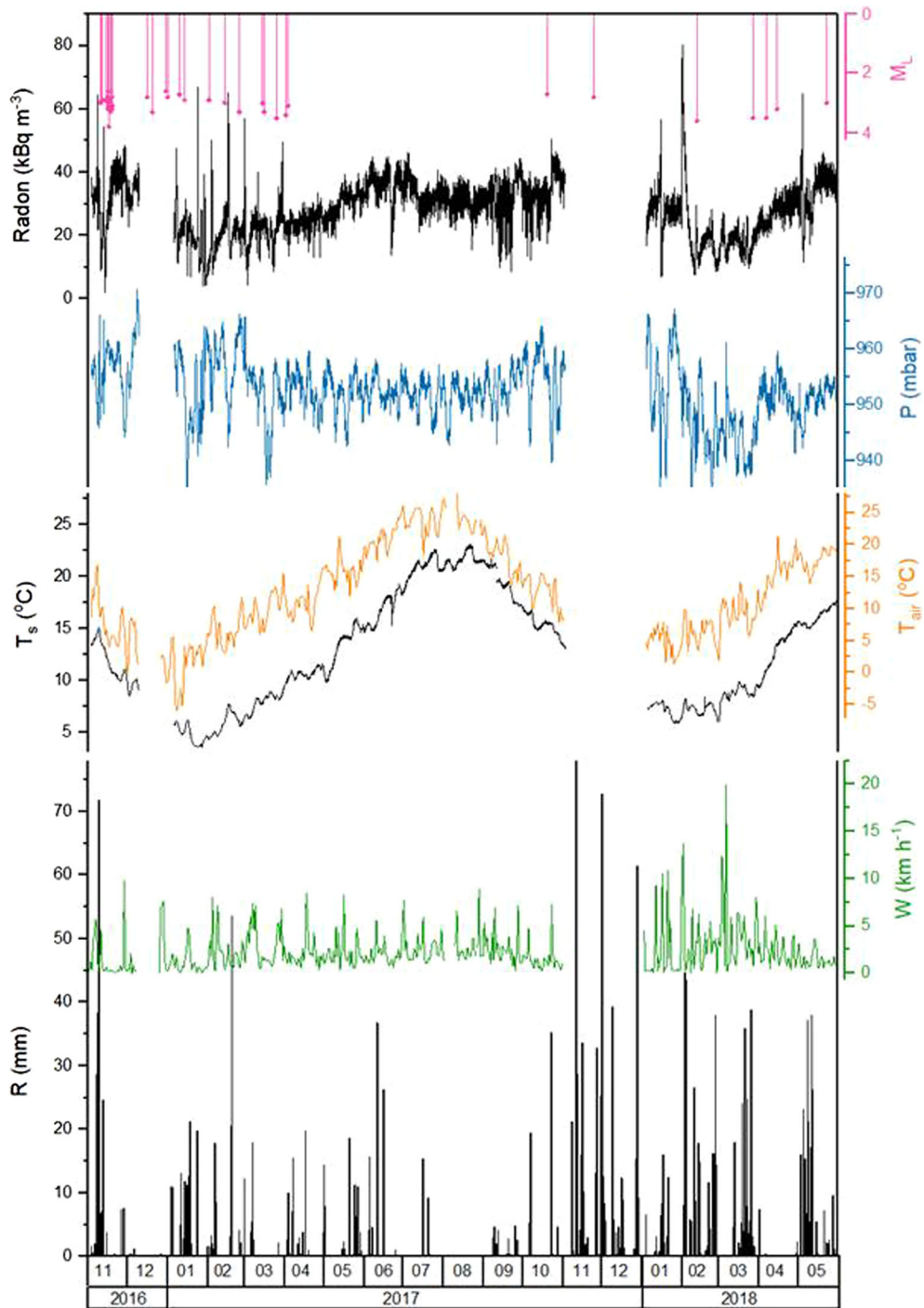


Figure 2

Temporal variations of soil radon concentration, atmospheric pressure ( $P$ ), soil temperature ( $T_s$ ), air temperature ( $T_{air}$ ), wind speed ( $W$ ) and rainfall ( $R$ ). The local magnitudes ( $M_L$ ) of the earthquakes listed in Table 1 are also included

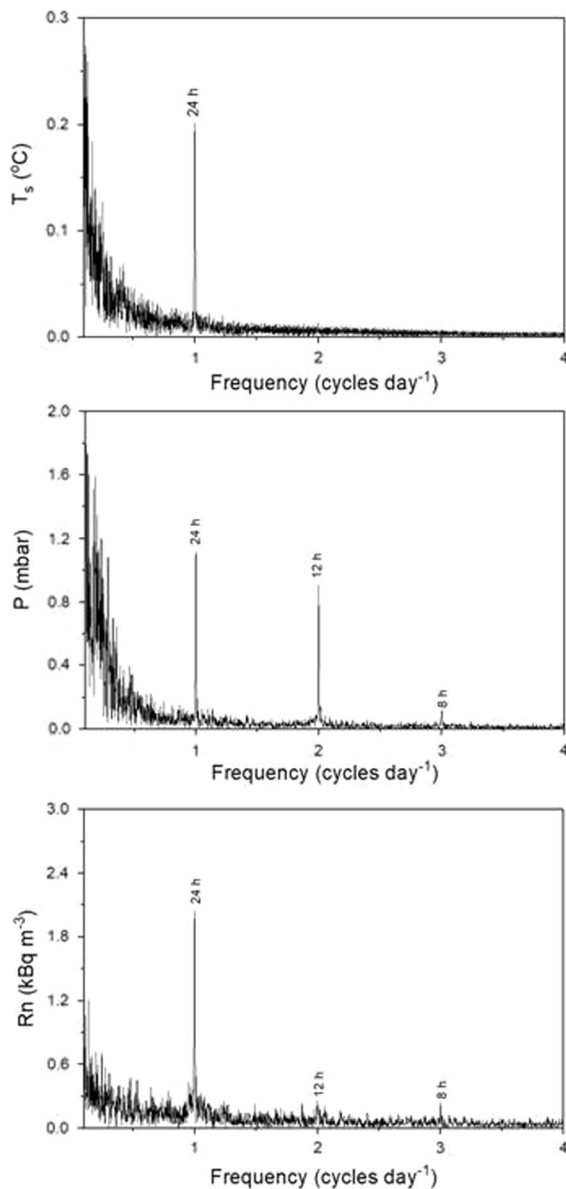


Figure 3

Fourier amplitude spectra calculated from soil temperature, atmospheric pressure and radon concentration data series, using a 1-h sampling rate

(Aumento 2002, Richon et al. 2009). These comparisons suggest that radon concentrations are chiefly affected by soil temperature, without ruling out the influence of atmospheric pressure variations.

The effect of additional meteorologic parameters—namely, air temperature ( $T_{\text{air}}$ ), rainfall ( $R$ ) and wind speed ( $W$ )—was examined by first computing daily averages of  $R_n$ ,  $P$  and  $T_s$  and then calculating

the partial correlation coefficients among the daily radon concentration and each of the recorded meteorologic parameters (Table 2). Since variations in meteorologic factors are interrelated, partial correlation allows examining the correlation of radon concentration with a certain meteorologic factor by eliminating the influence of contemporary variations in the other meteorologic factors. A strong positive partial correlation was observed between  $R_n$  and  $T_s$  ( $r = 0.609$ ,  $p = 0.000$ ) and between  $R_n$  and  $T_{\text{air}}$  ( $r = 0.501$ ,  $p = 0.000$ ), while a weaker positive partial correlation was observed between  $R_n$  and  $P$  ( $r = 0.137$ ,  $p = 0.002$ ). No statistically significant correlation was observed with rainfall ( $r = -0.046$ ,  $p = 0.307$ ) and wind speed ( $r = -0.113$ ,  $p = 0.016$ ). The results confirm that soil radon concentrations are mainly influenced by  $T_s$  and to a lesser extent by  $P$ , as already indicated by the FFT analysis.

Particular attention has been paid to examining the effect of rainfall on radon time series, as striking similarities have been reported between rainfall- and earthquake-induced fluctuations in radon profile (Ramola et al. 2008; Walia et al. 2009, 2013; Fu et al. 2009, 2017a; Arora et al. 2017). In principle, rainfall events are expected to exert an impact on measured radon concentrations by affecting soil moisture levels. It is well known that radon emanation from soil and rock grains is enhanced at low-to-moderate moisture levels and hampered at increasing moisture levels (Tanner 1964). At the same time, depending on the soil attributes, water tends to reduce soil porosity and thus soil gas permeability, causing a reduction in radon transport (Megumi and Mamuro 1973; Lindmark and Rosen 1985). On the other hand, upon water saturation of the uppermost soil layers, the so-called capping mechanism may prevail—i.e., the formation of a capping layer blocks radon release into the atmosphere and forces radon to concentrate beneath the soil surface. As a result, an increase in measured soil-gas radon concentrations may be observed following heavy rainfall (Lindmark and Rosen 1985; Schumann et al. 1989, 1994; Ramola et al. 2008). In all cases, soil radon concentrations should respond to rainfall events after a certain time lag, which depends on the type of soil/rock making up the geology of the investigated site, and thus cross correlation between the two time series is more

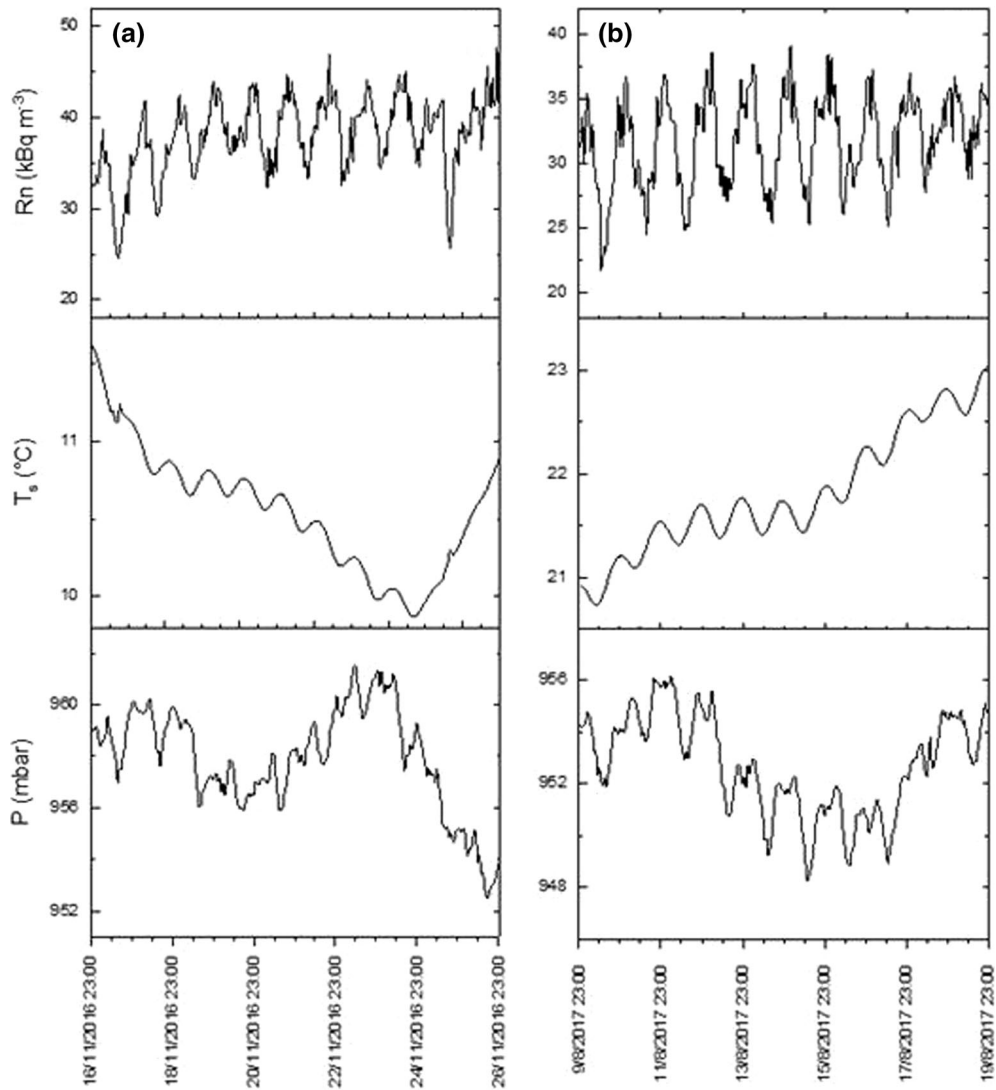


Figure 4

Diurnal variations of radon concentration, soil temperature and atmospheric pressure for the periods **a** 17–27 November 2016 and **b** 10–20 August 2017

Table 2

Partial correlation coefficients between soil radon concentrations and meteorologic parameters (*p* values are shown in parentheses). Statistically significant correlations (at the 0.05 level) are indicated with an asterisk

	Rn	$T_s$	$P$	$T_{air}$	$R$	$W$
Rn	1					
$T_s$	0.609* (0.000)	1				
$P$	0.137* (0.002)	0.034 (0.437)	1			
$T_{air}$	0.501* (0.000)	0.924* (0.000)	− 0.001 (0.974)	1		
$R$	− 0.046 (0.307)	− 0.143* (0.002)	− 0.156* (0.000)	− 0.135* (0.003)	1	
$W$	− 0.113 (0.016)	− 0.014 (0.758)	− 0.160* (0.000)	0.092 (0.051)	0.135* (0.004)	1



appropriate for detecting possible correlation between the two variables.

Cross-correlation analysis has been performed for the periods of undisrupted radon data, namely from 3 November 2016 to 9 December 2016, from 27 December 2016 to 2 November 2017 and from 4 January 2018 to 30 May 2018. The cross correlogram for the longest time series (from 27 December 2016 to 2 November 2017) is shown in Fig. 5. Although the cross-correlation coefficient is low, a maximum (absolute) value outside the 95% confidence interval was found to occur at lag  $-2$ , implying that radon concentrations decrease after a time lag of approximately 2 days following rainfall occurrence. Similar time lags, from  $-2$  to  $-4$ , were obtained for the other two time series. Shifting the rainfall time series backwards by a 2-day interval, the partial correlation between the radon concentration and rainfall remained statistically nonsignificant. Therefore, the effect of rainfall was neglected in the next step, and only  $T_s$ ,  $T_{air}$  and  $P$  were considered as controlling variables for predicting radon concentrations.

As the daily values of  $T_s$  and  $T_{air}$  showed a high positive correlation ( $r = 0.924$ ,  $p = 0.000$ ), it was decided to consider only  $T_s$  in the last step. A linear regression analysis was thus performed using the hourly  $T_s$  ( $^{\circ}\text{C}$ ),  $P$  (mbar) and  $\text{Rn}$  ( $\text{Bq m}^{-3}$ ) data from the Barasol probe, and the best regression model ( $R^2 = 0.433$ ) was determined as:

$$\text{Rn}_{\text{pred}} = 18534 + 841.0 \times T_s - 1.26 \times P.$$

The radon concentrations predicted by the above equation ( $\text{Rn}_{\text{pred}}$ ) were subsequently subtracted from the raw radon data, and the residual radon concentrations ( $\text{Rn}_{\text{res}}$ ) were obtained.

#### 4.2. Identification of Radon Anomalies

To discriminate between background and anomalous values, a probability analysis based on normal distribution plots was carried out in the residual radon time series (Fig. 6). The distribution of  $\text{Rn}_{\text{res}}$  values (practically 98%) lies on a nearly straight line, indicating that the population follows the normal distribution—i.e., radon variations are related to background radon fluctuations and fluctuations caused by environmental factors. One main inflection point is observed at  $\sim 15 \text{ kBq m}^{-3}$ , suggesting that  $\text{Rn}_{\text{res}}$  concentrations exceeding this value depart from normality.

The time series of  $\text{Rn}_{\text{res}}$  data is plotted in Fig. 7 together with the seismic events for selected time windows, covering the entire monitoring period. Although the correlation analysis of the whole data series showed that the radon concentration is not significantly influenced by rainfall, rainfall records are included in Fig. 7, as they may contribute to the interpretation of the observed radon fluctuations in the short time scale. The mean  $\text{Rn}_{\text{res}}$  value and  $\pm 2\sigma$

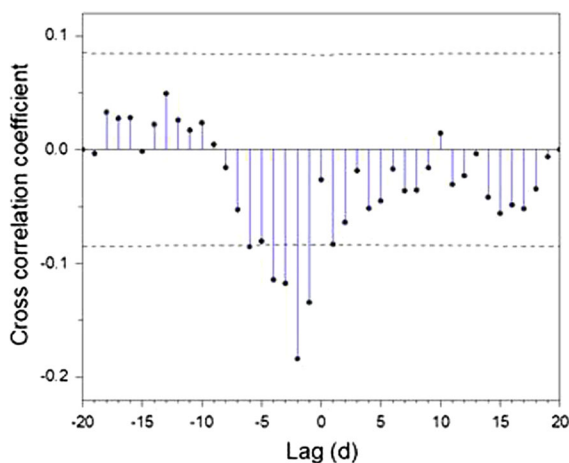


Figure 5

Cross correlation of radon concentration and rainfall time series for the time window from 27 December 2016 to 2 November 2017

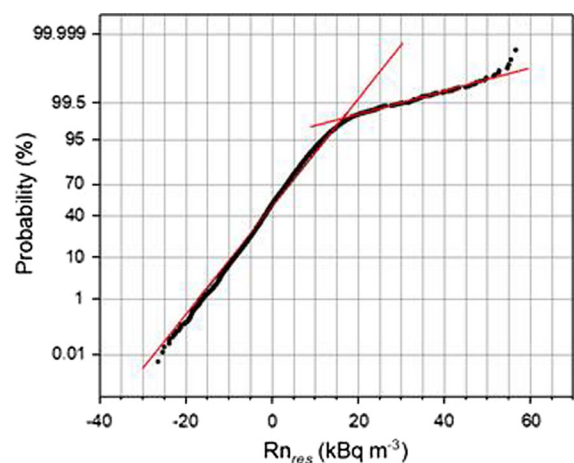
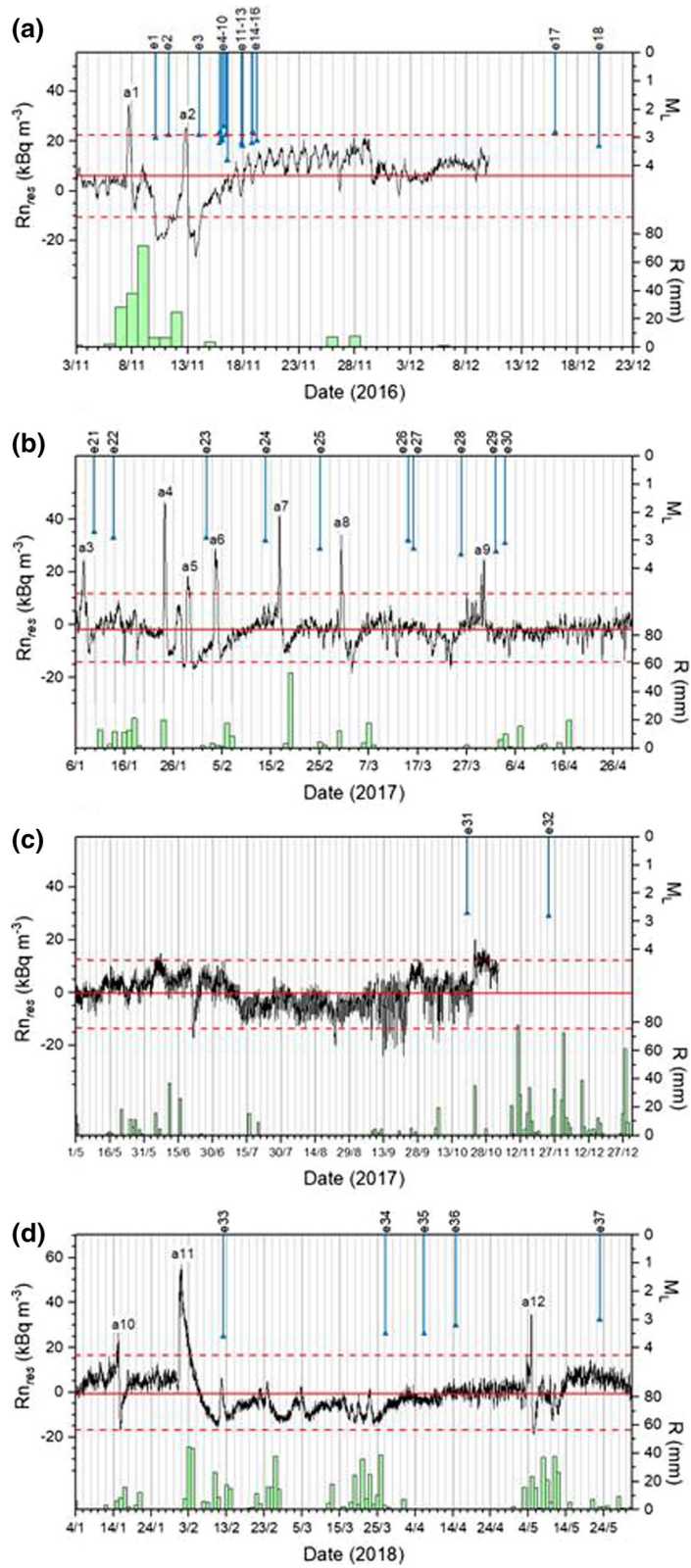


Figure 6

Normal probability plot of  $\text{Rn}_{\text{res}}$  values, revealing the presence of three distinct populations



◀Figure 7

The time series of residual radon concentrations ( $R_{n_{res}}$ ) in consecutive time windows. The mean  $R_{n_{res}}$  and  $\pm 2\sigma$  deviation from the mean are indicated by solid and dashed lines, respectively. The magnitude of earthquakes ( $M_L$ ) and the daily rainfall data ( $R$ ) are also plotted

deviation from the mean were calculated for each time window, as shown in Fig. 7. Values crossing the  $2\sigma$  deviations can be considered anomalies, possibly associated with seismic events in the study area. To facilitate the discussion, radon anomalies and earthquake events are denoted as  $a_i$  and  $e_i$ , respectively (see also Table 1).

Inspection of Fig. 7a reveals a period of anomalous radon signals from 7 to around 16 November 2016, initiated by a sudden increase in radon concentration that generated a sharp peak above the  $2\sigma$  deviation from the mean on 7 November 2016 (a1). Although afterwards radon seems to return to background levels, a significant drop occurs from 9 to 11 November 2016 and a second positive peak appears on 12 November 2016 (a2), followed by a decrease on 13–14 November 2016. Concentrations gradually return to background levels by 16 November 2016. According to the earthquake database, enhanced seismic activity was recorded during this period; seismic events occurred on 10, 11 and 13 November 2016 (e1, e2 and e3). A seismic swarm composed of seven earthquakes ( $M_L$  between 2.6 and 3.8) occurred within a  $< 24$  h period, from 15 to 16 November 2016 (e4–e10), at around 21 km from the monitoring site. Another six earthquakes ( $M_L$  max 3.3) occurred between 17 and 19 November 2016 (e11–e16) at the same epicenter. Radon concentrations returned to background levels during the remaining period up to 9 December 2016, which was free of earthquakes. The lack of radon data beyond 10 December 2016 does not allow any inferences for possible precursory signals associated with the earthquakes that occurred toward the end of December 2016 (e17–e20). Assigning the above radon anomalies to individual earthquakes is not straightforward because of the large number of closely occurring seismic events. However, it can be postulated that these anomalous radon signals, spreading from 7 to 16 November 2016, are

precursors of the seismic events recorded from 10 to 19 November 2016. The rationale adopted for an anomaly–earthquake association is discussed in the following section. It is worth noting that all earthquake events, with the exception of e1, in this time window originated from the fault zone that gave rise to the main shock of 15 October 2016.

At this point, it is noteworthy that heavy rainfall (28–72 mm) occurred on 7, 8 and 9 November 2016 and might be associated with the profile of radon between the a1 and a2 anomalies. Previously published studies have reported the occurrence of radon peaks induced by rainfall events. Müllerová et al. (2014) observed an increase in radon approximately 1 day and 5 days after precipitation for measurements performed at a depth of 0.4 m and 0.8 m, respectively. Radon peaks were detected with a time lapse of 12–18 h following rainfall sequences by Arora et al. (2017). Barkat et al. (2018) reported that the radon concentration was enhanced with a certain time lag at the onset of rain. Nevertheless, this does not seem to be the case in the present study. Keeping in mind that the radon concentration was found to be negatively cross correlated with rainfall with a time lag of approximately 2 days, it is reasonable to assume that the significant drop in radon concentration from 9 to 11 November 16 was caused by the high soil moisture content. A similar effect was reported by Piersanti et al. (2016) who observed that radon concentrations fall drastically by a factor  $> 10$  up to a factor of almost 100 after major precipitation episodes.

During the period from January to April 2017 displayed in Fig. 7b, a series of anomalous radon peaks appear. The anomaly on 7 January 2017 (a3) was followed by two earthquakes that occurred on 9 (e21) and 13 January 2017 (e22). However, radon data prior to 6 January 2017 are missing, and thus there is no information on whether another radon anomaly might be associated with these two seismic events. Radon peaks on 24 (a4) and 29 January 2017 (a5) were recorded prior to the earthquake of 1 February 2017 (e23). The anomalies on 3 (a6) and 16 February 2017 (a7) may serve as geochemical transients for the earthquakes on 13 (e24) and 24 February 2017 (e25), respectively. The earthquakes that occurred on 15 (e26) and 16 March 2017 (e27)

were preceded by a radon peak on 1 March 2017 (a8), while the earthquake of 25 March 2017 (e28) does not correlate with any radon peak. The last anomaly in this time window was observed on 30 March 2017 (a9) and was followed by earthquakes on 1 (e29) and 3 April 2017 (e30). Throughout this time window, mostly light-to-moderate rainfall was recorded, which does not seem to affect the radon profile.

The period from May to December 2017 (Fig. 7c) was seismically silent, with the exception of two earthquakes, on 20 October 2017 (e31) and 25 November 2017 (e32). No radon anomalies were observed during these months.

In the last time window (Fig. 7d), the anomaly observed at around 16 January 2018 (a10) is not likely correlated with any earthquake. The intense radon peak (a11) recorded on 1 February 2018 was followed by an earthquake on 12 February 2018 (e33). Concentrations remained below background levels for approximately 2 months following this peak. The latter might be associated with prolonged, heavy rainfall events that took place during this period. The seismic events that occurred on 27 March (e34), 6 April (e35), 15 April 2018 (e36) and 23 May 2018 (e37) were not preceded by any radon anomalies. By visual examination of the rainfall time series, it may be inferred that any rainfall-induced radon fluctuations are confined within the  $2\sigma$  deviation band. The radon peak detected on 4 May 2018, which marginally crosses the  $2\sigma$  band, was not considered to be an anomaly as it was accompanied by a prolonged period of rainfall.

#### 4.3. Radon Anomalies' Attributes and Association to Earthquakes

A critical issue in precursor studies is the association of radon anomalies to earthquake events. The selection of the earthquake that "corresponds" to a certain radon anomaly may be less straightforward than the definition of the radon anomaly itself. In published literature, a 1:1 approach, i.e., relating one radon anomaly to one earthquake, is by far the most popular procedure, albeit sometimes an arbitrary one (Hartmann and Levy 2005; Woith 2015). In the present study, there are cases where one anomaly is followed by several earthquakes (e.g., a1 and e3–e16)

and cases where one earthquake is preceded by more than one anomaly (e.g., e21–e22 and a3). In an attempt to establish an anomaly-earthquake association and given that only the magnitudes and epicentral distances were known for the considered earthquakes, the Dobrovolsky's earthquake preparation zone (Dobrovolsky et al. 1979) was used as an estimator of the strain impact at the monitoring site. The fact that a small-magnitude seismic event close to the monitoring site might have the same strain impact as a large-magnitude event at a greater distance was considered to reflect on the ratio  $R_E/R_D$  (Table 1). Radon anomalies were thus associated with the earthquake characterized by the lower  $R_E/R_D$  ratio (high magnitude, small epicentral distance).

In view of the above, the following associations were established and are marked in Table 1: a1–e1, a2–e10, a3–e22, a4/a5–e23, a6–e24, a7–e25, a8–e27, a9–e29 and a11–e33. Overall, 10 of the 11 observed radon anomalies might be associated with at least one earthquake event, while only 6 of 32 earthquake events (taking into account the periods of missing radon data) are likely not associated with any radon anomaly. It is interesting to remark that most of the events (e28, e31, e34, e35 and e37) that were not preceded by a radon anomaly occurred SSW of the city of Ioannina (see Fig. 1). Although the monitoring station was located within the probable preparation zone of the earthquakes, their particular geologic and

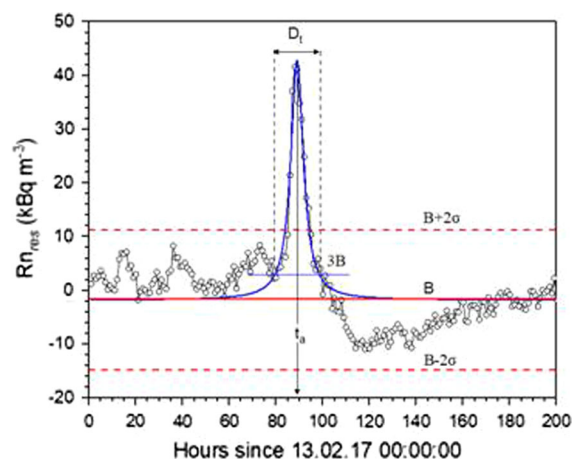


Figure 8  
Peak shape analysis of the a7 radon anomaly (16.2.17). The time ( $t_a$ ) the anomaly occurred and duration ( $D_t$ ) of the anomaly are determined by fitting a Lorentzian function to the radon data

tectonic environment, which affects stress transfer and strain accumulation, might explain the absence of associated radon anomalies.

The peak profile of radon anomalies was further analyzed to obtain the precursor time and anomaly duration. Following Hauksson (1981), the precursor time is defined as the time period from the onset of anomalous radon activity until the time of the earthquake occurrence. The anomaly duration was estimated by Igarashi and Wakita (1990) as the time period for which the radon concentration crosses the  $2\sigma$  interval from the corresponding seasonal mean. Depending on the radon peak profile, the above attributes may be determined in a quite subjective

manner, which is mostly based on visual analysis of the observed anomalies. According to Friedmann (2012), radon anomalies can be classified in two categories: “type A” anomalies, which are characterized by a rather slow change in radon concentration and can continue even over years, and “type B” anomalies, which appear as short peaks of hours to days duration and can be followed by a slow increase or a rather constant radon concentration. All radon anomalies detected in the present study can be classified as “type B” anomalies, initiated by a very fast increase from background level, followed by a similarly fast decrease, typically below background. To determine the duration ( $D_r$ ) of

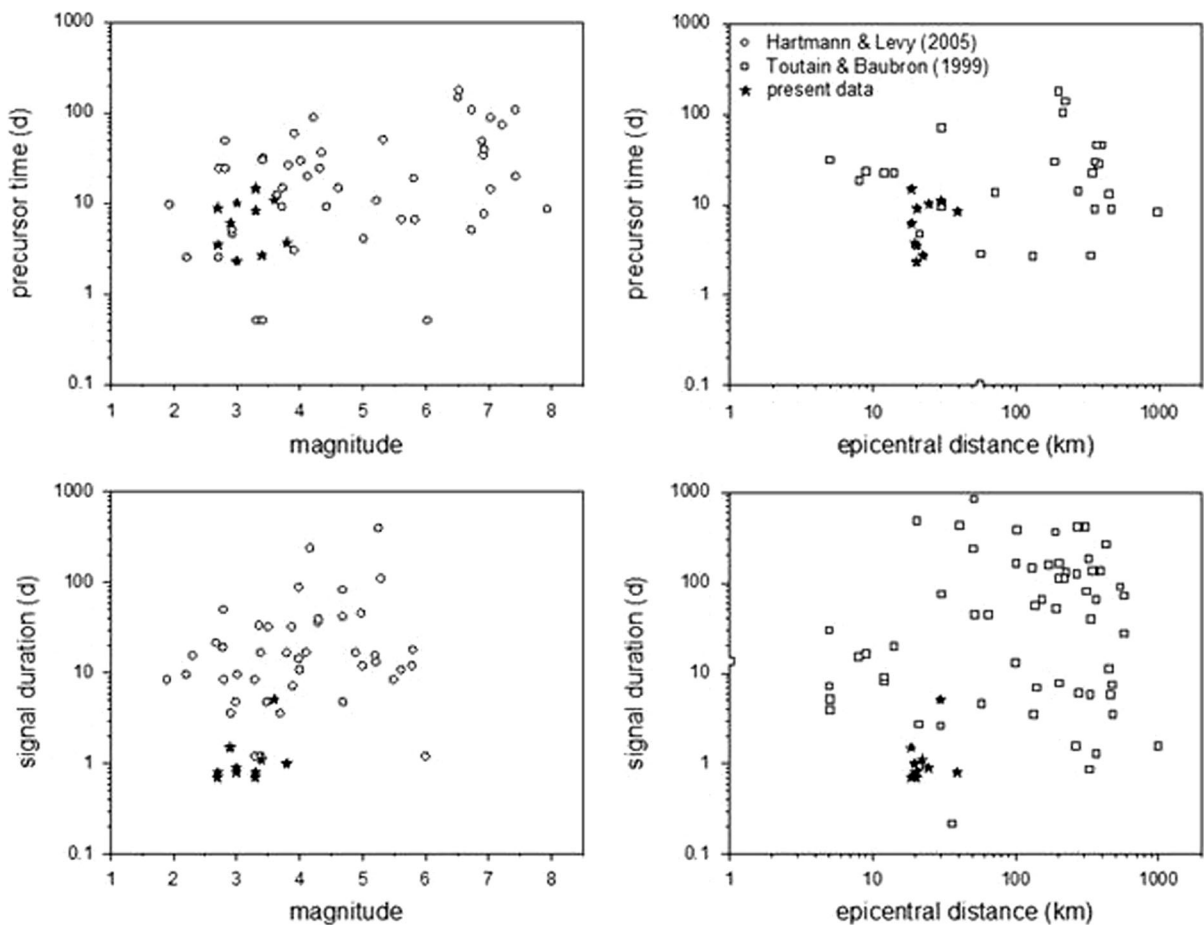


Figure 9

Scatter plots showing the relationship of earthquake magnitude and epicentral distance with the precursor time and signal duration of the radon anomalies. Literature data compiled by Toutain and Baubron (1999) and Hartmann and Levy (2005) are also plotted for comparison (only data applying to soil radon measurements have been graphically extracted from their compilations)

the anomaly and the time ( $t_a$ ) the anomaly occurred, either a Gaussian or a Lorentzian function was fitted to each of the anomalous radon peaks. An example of a Lorentzian function fit is given in Fig. 8 for the anomaly a7, detected on 16 February 2017. By fixing the vertical offset to the  $Rn_{res}$  background level (B) previously determined for the corresponding time window,  $D_t$  is calculated as the time duration for which the peak crosses the 3B level. The time occurrence ( $t_a$ ) corresponds to the center of the Lorentzian, and the precursor time ( $t_p$ ) is obtained as the time difference between the peak of the anomaly ( $t_a$ ) and the earthquake event ( $t_e$ ). For the case of Fig. 8, the peak occurred on 16 February 2017 16:00:00—i.e., the a7 anomaly preceded the e25 earthquake by 8.3 days and had a 20-h duration. By applying the same analysis to all anomalous radon peaks, the parameters  $t_a$ ,  $t_p$  and  $D_t$  were derived, as listed in Table 1.

The above findings were compared with worldwide data, relevant to soil radon measurements, graphically presented in the reviews by Toutain and Baubron (1999) and Hartmann and Levy (2005). Scatter plots showing the relationship of earthquake magnitude and epicentral distance with the precursor time and signal duration of radon anomalies are displayed in Fig. 9. Naturally, the seismic events considered in the present study cover only a small range of magnitudes and epicentral distances. The precursor times span from 2.3 to 14.7 days is within the range of values reported by other studies. Concerning anomaly durations, the present values—between 0.7 and 5.1 days—lie toward the lower end of published values. This may partly originate from the fact that the present data are based on hourly recordings, whereas the data compiled by Toutain and Baubron (1999) and Hartmann and Levy (2005) are mostly based on measurements integrated over longer time periods. Radon peak durations down to 0.21 days have been recently reported by Fu et al. (2017b).

### 5. Conclusions

Soil gas radon was continuously monitored along with meteorologic parameters from November 2016

to May 2018 near a seismically active location in the area of Ioannina (Epirus, Northwestern Greece). Partial correlation and cross-correlation analysis of radon and meteorologic data time series showed a strong positive correlation between radon concentration and soil/air temperature and a weaker positive correlation between radon concentration and atmospheric pressure. The effect of rainfall and wind speed was found to be statistically nonsignificant. Soil temperature and atmospheric pressure were included as explanatory variables in a multiple linear regression model to predict meteorologically driven radon variations. The residual radon time series was therefore considered to contain earthquake-driven variations. Based on the  $2\sigma$  deviation criterion, 11 spike-like radon anomalies were identified throughout the monitoring period. Searching for possible anomaly-earthquake associations, 37 seismic events were selected adopting Dobrovolsky's radius approach, and the following observations were made: (1) in most cases, a single radon anomaly was followed by several closely occurring earthquakes, (2) in some cases, a single anomaly was followed by a single earthquake, (3) in some cases, earthquakes were not related with any anomaly, (4) in one case, a single earthquake was preceded by more than one anomaly, and (5) in one case, the anomaly was not related to any earthquake. To obtain an anomaly-earthquake association, Dobrovolsky's earthquake preparation zone was used, and 10 of 11 observed radon anomalies were interpreted as precursors to at least one earthquake event. Analyzing the peak profile of radon anomalies, precursor times ranging from 2.3 to 14.7 days and anomaly durations ranging from 0.7 to 5.1 days were obtained.

### Acknowledgements

The authors express their gratitude to the two anonymous reviewers for their valuable comments and suggestions that improved the manuscript.

**Publisher's Note** Springer Nature remains neutral with regard to jurisdictional claims in published maps and institutional affiliations.

## REFERENCES

- Arora, B. R., Kumar, A., Walia, V., Yang, T. F., Fu, C.-C., Liu, T.-K., et al. (2017). Assessment of the response of the meteorological/hydrological parameters on the soil gas radon emission at Hsinchu, northern Taiwan: A prerequisite to identify earthquake precursors. *Journal of Asian Earth Sciences*. <https://doi.org/10.1016/j.jseae.2017.06.033>.
- Aubouin, J. (1959). Contribution à l'étude géologique de la Grèce, septentrionale: les confins de l'Épire et de la Thessalie. *Annales Géologiques des Pays Helléniques*, 10, 1–483.
- Aumento, F. (2002). Radon tides on an active volcanic island: Terceira, Azores. *Geofísica Internacional*, 41(4), 499–505.
- Barkat, A., Ali, A., Hayat, U., Crowley, Q. G., Rehman, K., Siddique, N., et al. (2018). Time series analysis of soil radon in Northern Pakistan: Implications for earthquake forecasting. *Applied Geochemistry*, 97, 197–208.
- Boccaletti, M., Caputo, R., Mountrakis, D., Pavlides, S., & Zouros, N. (1997). Paleoseismicity of the Souli fault, Epirus, Western Greece. *Journal of Geodynamics*, 24, 117–127.
- Cicerone, R. D., Ebel, J. E., & Britton, J. (2009). A systematic compilation of earthquake precursors. *Tectonophysics*, 476(3–4), 371–396.
- Dobrovolsky, I. P., Zubkov, S. I., & Miachkin, V. I. (1979). Estimation of the size of earthquake preparation zones. *Pure and Applied Geophysics*, 117(5), 1025–1044.
- Etioppe, G., & Martinelli, G. (2002). Migration of carrier and trace gases in the geosphere: an overview. *Physics of the Earth and Planetary Interiors*, 129(3–4), 185–204.
- Fleischer, R. L. (1981). Dislocation model for radon response to distant earthquakes. *Geophysical Research Letters*, 8(5), 477–480.
- Friedmann, H. (2012). Radon in earthquake prediction research. *Radiation Protection Dosimetry*, 149(2), 177–184.
- Fu, C.-C., Walia, V., Yang, T. F., Lee, L.-C., Liu, T.-K., Chen, C.-H., et al. (2017a). Preseismic anomalies in soil-gas radon associated with 2016 M6.6 Meinong earthquake, Southern Taiwan. *Terrestrial, Atmospheric and Oceanic Sciences*, 28(5), 787–798.
- Fu, C.-C., Yang, T. F., Chen, C.-H., Lee, L.-C., Wub, Y.-M., Liu, T.-K., et al. (2017b). Spatial and temporal anomalies of soil gas in northern Taiwan and its tectonic and seismic implications. *Journal of Asian Earth Sciences*, 149, 64–77.
- Fu, C.-C., Yang, T. F., Tsai, M. C., Lee, L. C., Liu, T. K., Walia, V., et al. (2017c). Exploring the relationship between soil degassing and seismic activity by continuous radon monitoring in the Longitudinal Valley of eastern Taiwan. *Chemical Geology*, 469, 163–175.
- Fu, C.-C., Yang, T. F., Walia, V., Liu, T.-K., Lin, S. J., Chen, C.-H., et al. (2009). Variations of soil-gas composition around the active Chihshang fault in a plate suture zone, eastern Taiwan. *Radiation Measurements*, 44(9–10), 940–944.
- Ghosh, D., Deb, A., Sahoo, S. R., Subrata, H., & Rosalima, S. (2011). Radon as seismic precursor: new data with well water of Jalpaiguri, India. *Natural Hazards*, 58(3), 877–889.
- Ghosh, D., Deb, A., & Sengupta, R. (2009). Anomalous radon emission as precursor of earthquake. *Journal of Applied Geophysics*, 69(2), 67–81.
- Gregorič, A., Zmazek, B., Dzeroski, S., Torkar, D., & Vaupotič, J. (2012). Radon as an earthquake precursor: methods for detecting anomalies. In S. D'Amico (Ed.), *Earthquake research and analysis: Statistical studies, observations and planning* (pp. 179–196). Rijeca: InTech. (ISBN: 978-953-51-0134-5).
- Hartmann, J., & Levy, J. K. (2005). Hydrogeological and gasgeochemical earthquake precursors—A review for application. *Natural Hazards*, 34(3), 279–304.
- Hatzfeld, D., Kassaras, I., Panagiotopoulos, D., Amorese, D., Makropoulos, K., Karakaisis, G., et al. (1995). Microseismicity and strain pattern in northwestern Greece. *Tectonics*, 14(4), 773–785.
- Hauksson, E. (1981). Radon content of groundwater as an earthquake precursor: evaluation of worldwide data and physical basis. *Journal of Geophysical Research*, 86(B10), 9397–9410.
- Hauksson, E., & Goddard, J. G. (1981). Radon earthquake precursor studies in Iceland. *Journal of Geophysical Research*, 86(B8), 7037–7054.
- Igarashi, G., & Wakita, H. (1990). Groundwater radon anomalies associated with earthquakes. *Tectonophysics*, 180(2–4), 237–254.
- Immè, G., & Morelli, D. (2012). Radon as earthquake precursor. In S. D'Amico (Ed.), *Earthquake research and analysis: Statistical studies, observations and planning* (pp. 143–160). Rijeca: InTech. (ISBN: 978-953-51-0134-5).
- Jaishi, H. P., Singh, S., Tiwari, R. P., & Tiwari, R. C. (2014). Analysis of soil radon data in earthquake precursory studies. *Annals of Geophysics*, 57(5), S0544. <https://doi.org/10.4401/ag-6513>.
- Karakitsios, V. (2005). The Ioannina karstic plateau and its water management. In *Proceedings of the 7th Hellenic Hydrogeological Conference*, Athens, 2005 (pp. 171–181) (in Greek). <https://doi.org/10.13140/2.1.4464.0009>.
- King, C. Y. (1986). Gas geochemistry applied to earthquake prediction. An overview. *Journal of Geophysical Research*, 91(B12), 12269–12281.
- King, G., Sturdy, D., & Whitney, J. (1993). The landscape geometry and active tectonics of northwest Greece. *Geological Society of America Bulletin*, 105(2), 137–161.
- Kristiansson, K., & Malmqvist, L. (1982). Evidence for nondiffusive transport of <sup>222</sup>Rn in the ground and a new physical model for the transport. *Geophysics*, 47(10), 1444–1452.
- Kumar, A., Walia, V., Arora, B., Yang, T., Lin, S.-J., Fu, C.-C., et al. (2015). Identifications and removal of diurnal and semidiurnal variations in radon time series data of Hsinhua monitoring station in SW Taiwan using singular spectrum analysis. *Natural Hazards*, 79(1), 317–330.
- Lindmark, A., & Rosen, B. (1985). Radon in soil gas—Exhalation tests and in situ measurements. *The Science of the Total Environment*, 45, 397–404.
- Matsumoto, N. (1992). Regression analysis of anomalous changes of ground water level due to earthquakes. *Geophysical Research Letters*, 19(12), 1193–1196.
- Megumi, K., & Mamuro, T. (1973). Radon and thoron exhalation from the ground. *Journal of Geophysical Research*, 78(11), 1804–1808.
- Mentes, G., & Eper-Pápai, I. (2015). Investigation of temperature and barometric pressure variation effects on radon concentration in the Sopronbámfalva Geodynamic Observatory, Hungary. *Journal of Environmental Radioactivity*, 149, 64–72.
- Müllerová, M., Holý, K., & Bulko, M. (2014). Daily and seasonal variations in radon activity concentration in the soil air. *Radiation Protection Dosimetry*, 160(1–3), 222–225.
- Negarestani, A., Setayeshi, S., Ghannadi-Maragheh, M., & Akashe, B. (2003). Estimation of the radon concentration in soil related to

- the environmental parameters by a modified Adaline neural network. *Applied Radiation and Isotopes*, 58(2), 269–273.
- Ntokos, D. (2017a). Neotectonic—Geomorphological study of Epirus, Northwestern Greece and Compiling of Neotectonic Map, by use of Geographic Information Systems, Ph.D. Thesis, National Technical University of Athens, (in Greek). <http://dspace.lib.ntua.gr/handle/123456789/44623>.
- Ntokos, D. (2017b). Synthesis of literature and field work data leading to the compilation of a new geological map—A review of geology of northwestern Greece. *International Journal of Geosciences*, 8(2), 205–236.
- Ntokos, D. (2018). Neotectonic study of Northwestern Greece. *Journal of Maps*, 14(2), 178–188.
- Oh, Y. H., & Kim, G. (2015). A radon-thoron isotope pair as a reliable earthquake precursor. *Scientific Reports*, 5, 13084. <https://doi.org/10.1038/srep13084>.
- Papazachos, B., & Papazachou, K. (1989). *The earthquakes of Greece*. Thessaloniki: Ziti editions. (in Greek).
- Pavlidis, S., Ganas, A., Chatzipetros, A., Sboras, S., Valkaniotis, S., Papanthanasou, G., et al. (2017). Geological and seismotectonic characteristics of the broader area of the October 15, 2016, earthquake (Ioannina, Greece). *Geophysical Research Abstracts*, 19, EGU2017-18135-1, EGU General Assembly.
- Pavlidis, S., Ganas, A., Papanthanasou, G., Valkaniotis, S., Thomaidou, E., Georgiadis, G., et al. (2016). Geological-seismotectonic study of the wider area of Ioannina (seismic region of the earthquake October 15, 2016). Tectonics & Structural Geology Committee of the Geological Society of Greece. 1st Tectonics and Structural Geology Meeting, Athens 6 December 2016. Available online at: [http://www.geosociety.gr/images/ImeridaTektonikis\\_2016/1st\\_TSG\\_Meeting\\_Proceedings\\_small.pdf](http://www.geosociety.gr/images/ImeridaTektonikis_2016/1st_TSG_Meeting_Proceedings_small.pdf). Accessed 17 April 2018.
- Pavlidis, S., Valkaniotis, S., & Chatzipetros, A. (2008). Seismically capable faults in Greece and their use in seismic hazard assessment. In *4th International Conference on Earthquake Geotechnical Engineering*, 25–28 June 2007, Thessaloniki, Proceedings, paper n. 1609.
- Petraki, E., Nikolopoulos, D., Panagiotaras, D., Cantzos, D., Yannakopoulos, P., et al. (2015). Radon-222: A potential short-term earthquake precursor. *Journal of Earth Science and Climatic Change*, 6, 282. <https://doi.org/10.4172/2157-7617.1000282>.
- Piersanti, A., Cannelli, V., & Galli, G. (2016). The Pollino 2012 seismic sequence: clues from continuous radon monitoring. *Solid Earth*, 7, 1303–1316.
- Ramola, R. C., Prasad, Y., Prasad, G., Kumar, S., & Choubey, V. M. (2008). Soil–gas radon as seismotectonic indicator in Garhwal Himalaya. *Applied Radiation and Isotopes*, 66(10), 1523–1530.
- Richon, P., Perrier, F., Pili, E., & Sabroux, J.-C. (2009). Detectability and significance of 12 h barometric tide in radon-222 signal, dripwater flow rate, air temperature and carbon dioxide concentration in an underground tunnel. *Geophysical Journal International*, 176(3), 683–694.
- Riggio, A., & Santulin, M. (2015). Earthquake forecasting: a review of radon as seismic precursor. *Bollettino di Geofisica Teorica ed Applicata*, 56(2), 95–114.
- Schumann, R. R., Gundersen, L. C. S., & Tanner, A. B. (1994). Geology and occurrence of radon. In N. L. Nagda (Ed.), *Radon: Prevalence, measurements, health risks and control*, ASTM Manual Series: MNL 15 (pp. 83–96). Philadelphia: American Society for Testing and Materials.
- Schumann, R. R., Owen, D. E., & Asher-Bolinder, S. (1989). Weather factors affecting soil–gas radon concentrations at a single site in the semiarid western US. In *Proceedings of the 1988 EPA Symposium on Radon and Radon Reduction Technology*, Vol. 2, Publication EPA/600/9-89/006B (pp. 3.1–3.13).
- Sikder, I. U., & Munakata, T. (2009). Application of rough set and decision tree for characterization of premonitory factors of low seismic activity. *Expert Systems with Applications*, 36(1), 102–110.
- Singh, M., Ramola, R. C., Singh, S., & Virk, H. S. (1988). The influence of meteorological parameters on soil–gas radon. *Journal of Association of Exploration Geophysicists*, 9(2), 85–90.
- Tanner, A. B. (1964). Radon migration in the ground: A review. In J. A. S. Adams & W. M. Lowder (Eds.), *The natural radiation environment* (pp. 161–190). Chicago: University of Chicago Press.
- Tomer, A. (2016). Radon as an earthquake precursor: A review. *International Journal of Science, Engineering and Technology*, 4(6), 815–822.
- Torkar, D., Zmazek, B., Vaupotič, J., & Kobal, I. (2010). Application of artificial neural networks in simulating radon levels in soil gas. *Chemical Geology*, 270(1–4), 1–8.
- Toutain, J.-P., & Baubron, J.-C. (1999). Gas geochemistry and seismotectonics: A review. *Tectonophysics*, 304(1–2), 1–27.
- Tselentis, G.-A., Sokos, E., Martakis, N., & Serpetsidaki, A. (2006). Seismicity and seismotectonics in Epirus, Western Greece: Results from a microearthquake survey. *Bulletin of the Seismological Society of America*, 96(5), 1706–1717.
- Vaupotic, J., Riggio, A., Santulin, M., Zmazek, B., & Kobal, I. (2010). A radon anomaly in soil gas at Cazzaso, NE Italy, as a precursor of an ML = 5.1 earthquake. *Nukleonika*, 55(4), 507–511.
- Virk, H. S., Sharma, A. K., & Sharma, N. (2002). Radon and helium monitoring in some thermal springs of North India and Bhutan. *Current Science*, 82(12), 1423–1424.
- Walia, V., Yang, T. F., Lin, S. J., Hong, W. L., Fu, C. C., Wen, K. L., et al. (2009). Continuous temporal soil gas composition variations for earthquake precursory studies along Hsincheng and Hsinhua faults in Taiwan. *Radiation Measurements*, 44(9–10), 934–939.
- Walia, V., Yang, T. F., Lin, S. J., Kumar, A., Fu, C. C., Chiu, J. M., et al. (2013). Temporal variation of soil gas compositions for earthquake surveillance in Taiwan. *Radiation Measurements*, 50, 154–159.
- Woith, H. (2015). Radon earthquake precursor: A short review. *European Physical Journal Special Topics*, 224(4), 611–627.
- Zmazek, B., Todorovski, L., Džeroski, S., Vaupotič, J., & Kobal, I. (2003). Application of decision trees to the analysis of soil radon data for earthquake prediction. *Applied Radiation and Isotopes*, 58(6), 697–706.
- Zmazek, B., Živčić, M., Todorovski, L., Džeroski, S., Vaupotič, J., & Kobal, I. (2005). Radon in soil gas: How to identify anomalies caused by earthquakes. *Applied Geochemistry*, 20(6), 1106–1119.